Using mutual information to determine geoeffectiveness of solar wind phase fronts with different front orientations

T. G. Cameron[1], B. Jackel[1], D. M. Oliveira[2,3]

T. G. Cameron, tgcamero@ucalgary.ca

[1]Department of Physics and Astronomy, University of Calgary, Calgary, Alberta, Canada.

[2]NASA Goddard Space Flight Center, Greenbelt, MD USA

[3]Goddard Planetary Heliophysics Institute, University of Maryland, Baltimore County, Baltimore, MD USA

This article has been accepted for publication and undergone full peer review but has not been through the copyediting, typesetting, pagination and proofreading process, which may lead to differences between this version and the Version of Record. Please cite this article as doi: 10.1029/2018JA026080

Abstract. The geoeffectiveness of solar wind shocks depends on angle with respect to the Sun-Earth line, with highly angled solar wind shocks being less geoeffective than nearly frontal solar wind shocks. However, it is unclear whether this holds for the orientation of structures in non-shocked solar wind. In this paper, we perform a mutual information analysis of 18 years of in-situ solar wind and ground magnetometer data in order to investigate the effects of solar wind phase front orientation on solar wind geoeffectiveness (indicated by SuperMAG SME). Since geomagnetic response is strongly influenced by Interplanetary Magnetic Field (IMF) B_z, and IMF B_z affects phase front orientation, we use conditional mutual information to account for the effect of B_z on geomagnetic activity. In contrast to what has been found for solar wind shocks, we find that during times of IMF $B_z > 0$, phase fronts aligned with the average Parker spiral direction (45 deg azimuth, 0 deg inclination) tend to be associated with higher geomagnetic activity (SME > 500 nT) than would be expected if IMF B_z and phase front orientation quantities were unrelated. During times of IMF $B_z < \ 0$, there is no connection between solar wind phase front orientation and geomagnetic activity (SME). We believe that Parker spiral aligned phase fronts being associated with higher geomagnetic activity during times of IMF $B_z > 0$ is due to constant phase front orientation allowing for more efficient energy transfer either through viscous interaction or high latitude reconnection.

Keypoints:

- Solar wind phase front orientation geoeffectiveness is quantified using information theory.
- When $B_z > 0$, solar wind phase fronts are more often highly geoeffective when aligned with the average Parker spiral direction.
- When $B_z < 0$, there is no connection between solar wind phase front orientation and solar wind geoeffectiveness.

1. Introduction

Geomagnetic activity occurring in near-Earth space is controlled primarily by the solar wind. Energy is transferred through the magnetosphere and to the ionosphere through a variety of mechanisms. When the solar wind magnetic field is directed primarily southward (IMF $B_z < 0$), a process called magnetic reconnection can occur at the magnetopause and in the magnetotail where the Earth's magnetic field merges with the Sun's, resulting in the transfer of large amounts of energy from the Sun to the Earth. When the solar wind magnetic field is directed northward (IMF $B_z > 0$), however, energy transfer is significantly reduced (eg. (Lu, Jing, Liu, Kabin, & Jiang, 2013)). During these times, energy is transferred to the magnetosphere though a combination of reconnection at high latitude (Crooker, 1992), and other mechanisms commonly referred to as "viscous interaction" (first introduced by (Axford, 1964)). It is clear that the solar wind magnetic field determines to a large degree the geoeffectiveness of the solar wind, that is, the amount of energy transferred from the solar wind to the Earth. What is less well known is to what extent geoeffectiveness depends on other properties of the solar wind, such as its spatial structure.

The solar wind is typically arranged in large planar structures with radii of curvature of at least 100s of R_e (R_e = 6371 km) (Lepping, Wu, & McCleman, 2003 ; Collier, Szabo, Slavin, & Lepping, 2000). The interplanetary magnetic field is embedded in these structures, which propagate with the solar wind flow away from the Sun towards the Earth. Although these phase fronts can be oriented in any direction, on average though

they tend to be oriented in the Parker spiral direction (Parker, 1965). This direction is given by

$$\phi_p = \frac{\Omega r}{v} \tag{1}$$

where Ω is the angular velocity of the Sun, r is the radial distance from the Sun, and v is the solar wind speed. Near Earth, for a typical value of $v \approx 400$ km/s, $\phi_p \approx 45$ degrees duskward from the Earth-Sun line on the ecliptic.

(Jurac & Richardson, 2001) examined solar wind structures as measured by four spacecraft over a solar cycle, and found that more geoeffective solar wind tended to have front normals arranged radially. There was no indication whether this was a causal relationship, or whether some other effect was behind this. Other than (Jurac & Richardson, 2001), to our knowledge, no special attention has been paid to geoeffectiveness controlled by the solar wind front angles as they interact with the magnetosphere.

However, in recent years, growing attention has been given to interplanetary (IP) shock orientation as a factor influencing how well the shock transfers energy to the magnetosphere (usually referred to as geoeffectiveness). For example, (Takeuchi, Russell, & Araki, 2002) showed that a gradual increase in the magnetospheric dynamic pressure was the result of the impact of an IP shock highly inclined in the equatorial plane. This result was later confirmed by simulations (Guo, Hu, & Wang, 2005 ; Selvakumaran, Veenadhari, Ebihara, Kumar, & Prasad, 2017) and observations (Wang, Li, Huang, & Richardson, 2006). (Oliveira & Raeder, 2014) conducted global MHD simulations to show that an inclined IP shock with high Mach number was much less geoeffective than an IP shock as half as weak which impacted the Earth frontally. These authors attributed this effect

to a much larger geoefficiency due to a symmetric compression in the second case. These results were later confirmed observationally by (Oliveira & Raeder, 2015) for substorm activity and by (Oliveira, Raeder, Tsurutani, & Gjerloev, 2016) for the nightside auroral power triggered by IP shocks with different orientations. Numerical simulations as conducted by (Samsonov, Sergeev, Kuznetsova, & Sibeck, 2015) showed that a highly inclined moderate IP shock compressed the magnetosphere asymmetrically which in turn led to overshoots in the horizontal geomagnetic field observed by artificial ground stations located in the magnetospheric flank opposite to the flank of impact. (Oliveira et al., 2018) showed that high-speed, nearly frontal shocks lead to intense dB/dt perturbations, which are associated with geomagnetically induced currents (GICs). They showed that such shocks can be associated with unusually high dB/dt variations at near-noon local time in magnetic equatorial regions due to strong enhancements of the equatorial electrojet current. (Oliveira & Samsonov, 2018) have recently provided a detailed review of geomagnetic activity triggered by shocks with different angles of impact.

As reported in the literature, the occurrence rate of IP shocks depends on solar activity with rates varying from less than 1 to 5 IP shocks per month (Kilpua, Lumme, Andreeova, Isavnin, & Koskinen, 2015 ; Oliveira & Raeder, 2015 ; Oliveira & Samsonov, 2018). From these statistics, it is clear that the solar wind is in a non-shocked state the vast majority of the time. Consequently, even a weak relationship between non-shocked solar wind orientation and geoeffectiveness could play a significant role in the geospace system.

In this paper, we studied solar wind geoeffectiveness as a function of solar wind phase front orientation using 18 years of spacecraft and ground magnetometer data. An enhanced version of the well-known AE index (Explained in Section 2.2) served as a geo-

magnetic activity indicator. Solar wind phase front orientation was determined using the MVAB-0 method, which is explained in Section 2.1. We carried out this analysis using the concept of pointwise mutual information which quantifies the relationship between two variables relative to the null hypothesis of independence, here represented by phase front orientation and geomagnetic activity. Since IMF B_z affects both phase front orientation (through the MVAB-0 method) and solar wind geoeffectiveness (through dayside and tail reconnection), we also used the related concept of pointwise conditional mutual information to isolate only the effect phase front orientation had on geoeffectiveness.

2. Data and Methods

2.1. Phase Front Normals

We start by describing the method used to estimate solar wind phase front orientation. With multiple satellites, simple geometry can be used to accurately compute solar wind phase front normals. However, this ideal configuration of solar wind probes is quite rare. For this paper we used the MVAB-0 (constrained minimum variance) method, which is explained in detail by (Sonnerup & Scheible, 1998). MVAB-0 uses the variation of single point IMF measurements to estimate phase front orientation. This is accomplished by first calculating the covariance matrix $M_{\mu\nu}$ (where μ and ν are arbitrary spatial indices) from solar wind IMF measurements.

$$M_{\mu\nu} = \langle B_\mu B_\nu \rangle - \langle B_\mu \rangle \langle B_\nu \rangle \tag{2}$$

A modified matrix $M^{**}_{\mu\nu}$ is then computed

$$M^{**}_{\mu\nu} = P_{\mu i} M_{ij} P_{j\nu} \tag{3}$$

with $P_{\mu\nu}$ defined as

$$P_{\mu\nu} = \delta_{\mu\nu} - \hat{B}_\mu \hat{B}_\nu, \tag{4}$$

where $\delta_{\mu\nu}$ is the Kronecker delta and the $\hat{B}$ is a unit vector in the average direction of the magnetic field for the entire interval. This matrix $M^{**}_{\mu\nu}$ yields three eigenvalues and eigenvectors. The smallest eigenvalue is zero, with the corresponding eigenvector pointing in the average magnetic field direction. The eigenvector corresponding to the next smallest eigenvalue is taken to be the phase front normal direction. Physically, this method finds the direction of least variance in IMF fluctuations perpendicular to the average magnetic field direction. In some cases the two non-zero eigenvalues are close in magnitude, and there isn't a clear normal vector. We used the standard criteria that the second smallest eigenvalue be at most half the largest eigenvalue to be accepted. Intervals where this was not the case were thrown out. The accuracy of this method for estimating solar wind phase front orientation has been established indirectly through its usefulness in calculating accurate solar wind time-shifts (Mailyan, Munteanu, & Haaland, 2008 ; Cameron & Jackel, 2016).

The IMF data used to estimate phase front orientation using MVAB-0 were obtained from the magnetometer (MAG) instrument onboard the Advanced Composition Explorer (ACE) spacecraft. We used two minute resolution data ranging from 1998 through 2015, splitting the data into one hour intervals separated by a half hour each. For each interval MVAB-0 was used to calculate a phase front orientation. Changing interval lengths ranging from 30 minutes to 2 hours were found to have very little bearing on the results. Intervals shorter than 30 minutes resulted in too few points for a good phase front normal determination, and much worse statistics. Intervals longer than two hours were too large

to capture variations in the solar wind. IMF B_z, solar wind number density, and solar wind speed were also obtained from ACE and averaged for each interval.

2.2. Geomagnetic Activity Indicator

Auroral substorm activity is often measured by ground magnetometers located in auroral zones as described by the well-known indices AU, AL, and AE = AU - AL, first suggested by (Davis & Sugiura, 1966). These indices correspond to the measurements of the upper auroral electroject (AU), the lower auroral electroject (AL), and their difference AE. Despite being widely used for many decades, these indices are not ideal for large statistical studies, as pointed out by (Oliveira & Raeder, 2015), because sometimes the limited number (10-12) of ground magnetometers is not enough to capture a significant portion of geomagnetic activity in the auroral zones around the world. In order to correct this deficiency, SuperMAG indices, computed by the SuperMAG project (Gjerloev, Hoffman, Friel, Frank, & Sigwarth, 2004), were used in this study. The SuperMAG indices are essentially the same as AE, AU, AL, but more than 500 magnetometers around the globe are used to compute them. Therefore, we used the SME index (the SuperMAG enhanced version of the AE index), to estimate geomagnetic activity in this study. (Newell & Gjerloev, 2011a, 2011b). Specifically, for each phase front normal, we recorded the maximum SME index in a 1 hour interval of time centered on some later time after the phase front normal time to allow for travel time from ACE to the magnetosphere. This lag time was calculated separately for each interval using a simple flat timeshift algorithm (ballistic propagation using ACE position and solar wind velocity on the Earth-Sun line). Similar to the ACE data, time intervals between a half hour and 2 hours had very little effect on the results, with intervals longer or shorter than that not capturing variations in geomag-

netic activity as well. Technical aspects of the SuperMAG data can be found in (Gjerloev, 2012). Data are readily available at the website `http://supermag.jhuapl.edu`.

2.3. Mutual Information

We considered approximately 300,000 one hour intervals from 1998 to 2015, each with a solar wind phase front normal ($\mathbf{n}$), IMF B_z, and lagged SuperMAG SME measurement. We threw out intervals that occurred within 6 hours of any solar wind shocks, using a list of shocks observed by solar wind spacecraft from 1995 to 2016. A version of this list up to 2013 is found in (Oliveira & Raeder, 2015). A simple linear correlation analysis (scatterplot, not shown) only displayed a very weak relationship between SME and phase front angle (from the Earth-Sun line). Pearson correlation coefficients (Table 1) are all less than 0.1 between the phase front orientation quantities and SME. In contrast the correlation coefficient is -0.36 between B_z and SME, suggesting that orientation effects are likely negligible compared to reconnection. However, correlation coefficients only detect linear relationships between quantities.

Our approach to exploring the relationship between these quantities was to consider quantities from information theory. Mutual information quantifies the amount of information shared by two random variables X and Y, and provides a more general measure of the relationship than the Pearson correlation. It is defined as

$$I(X;Y) = \sum_{y \in Y} \sum_{x \in X} p(x,y) \log_2 \left(\frac{p(x,y)}{p(x)p(y)} \right). \tag{5}$$

Lowercase x and y respectively refer to specific values of X and Y, while p(x) refers to the probability distribution of X and p(x,y) is the joint probability distribution of X

and Y. Mutual information has been used before in space physics to explore substorm reccurence (Prichard, Borovsky, Lemons, & Price, 1996), triggering (Johnson & Wing, 2014), and magnetospheric dynamics (Chen, Sharma, Edwards, Shao, & Kamide, 2008). In (Prichard et al., 1996) and (Chen et al., 2008), mutual information was used to explore temporal dynamics for time series at different lag times.

Mutual information can be useful as an integrated measure of how connected two quantities are, but sometimes it would be helpful to ask questions about the relationship between specific values of these two quantities. A tool for doing just that is called pointwise mutual information (PMI), sometimes called local mutual information (Lizier, 2014). PMI is defined so that mutual information is the expected value of pointwise mutual information. Therefore,

$$PMI(x;y) = \log_2\left(\frac{p(x,y)}{p(x)p(y)}\right). \tag{6}$$

PMI allows us to ask whether some pair of values of x and y occur together more or less often than what would be expected if their distributions were independent. If X and Y were independent, then PMI would be zero for all x and y. If we know PMI (in bits) for some x and y, then we know that 2^{PMI} times more events occurred for that x and y than if the two distributions were independent. In our case, we can obtain $p(x)$ and $p(y)$ from one dimensional histograms of our variables, and $p(x,y)$ from the two dimensional joint histogram. While mutual information allows us to explore connections between variables that simple correlation would miss, PMI allows us to be even more granular in our analysis.

For example, Fig. 1 shows the pointwise mutual information shared between IMF B_z and SME, for the 300,000 intervals described above. We can see that for intervals where

$B_z < 0$, large positive PMI (> 1) is present at increasing SME as B_z decreases. This large positive PMI means that in these parts of the SME - B_z distribution, we see more than twice ($> 2^1$) the number of intervals with these SME-B_z pairs than would be expected if the two quantities were independent. Conversely, we see very negative PMI (< 1) for intervals with low SME and large negative B_z. This means there were less than half ($< 2^{-1}$) the events with these B_z - SME pairs than would be expected if SME and IMF B_z were independent. If we now look at $B_z > 0$, the behavior is different. There is large negative PMI (< -0.5) for large SME events with any IMF B_z, and large positive PMI (> 0.5) for low SME events with any IMF B_z. This difference in behavior for positive and negative B_z is clearly due to the different mechanisms involved in energy transfer, and would not have been apparent if we only examined total mutual information.

2.4. Conditional Mutual Information

A problem that crops up often in multi-variable analysis is that of confounding variables. When investigating the relationship between X and Y, it might be that any connection found is simply the result of a third variable Z controlling both. One way we can account for this is to consider conditional mutual information, which quantifies the amount of information shared between two random variables (X and Y) that is not also shared with a third (Z). It is defined as (Wyner, 1978),

$$I(X;Y|Z) = I(X;Y,Z) - I(X;Z) = \sum_{z\in Z}\sum_{y\in Y}\sum_{x\in X} p(x,y,z)\log_2\left(\frac{p(z)p(x,y,z)}{p(x,z)p(y,z)}\right). \quad (7)$$

If Z is completely independent of X and Y, then this quantity becomes just the mutual information. Conversely, if the information shared between two variables (X and Y) is also

completely shared with a third (Z), such that $I(X;Y,Z) = I(X;Z)$, then this quantity sums to zero. Fig. 2 shows an illustration of how conditional mutual information is related to other informational quantities. Each circle represents the total information contained in a single random variable, while the various overlaps correspond to mutual information between them. In this way, we can show that $I(X;Y|Z)$ is the information shared between X and Y excluding the information that is also shared with Z. Using the diagram, it is also possible to see intuitively how $I(X;Y,Z) - I(X;Z) = I(X;Y|Z)$. (Johnson & Wing, 2014) and (Prichard et al., 1996) both used this quantity, which they referred to as conditional redundancy. (Prichard et al., 1996) used conditional mutual information to investigate if substorm recurrence can be predicted from previous substorms, while (Johnson & Wing, 2014) used it to compare different possible triggers for substorms.

In the same fashion as pointwise mutual information, we can define a quantity called pointwise conditional mutual information (PCMI), so that conditional mutual information is the expected value of this quantity. We can write it as follows,

$$PCMI(x;y|z) = \log_2\left(\frac{p(z)p(x,y,z)}{p(x,z)p(y,z)}\right). \tag{8}$$

For our purposes we do not consider the specific value of Z, and instead want a two dimensional (x and y) quantity to work with. We sum PCMI over z, weighted by p(z), to get

$$SPCMI(x;y|Z) = \sum_{z\in Z} p(z)PCMI(x;y|z) = \sum_{z\in Z} p(z)\log_2\left(\frac{p(z)p(x,y,z)}{p(x,z)p(y,z)}\right). \tag{9}$$

This quantity, which we call summed pointwise conditional mutual information (SPCMI), measures how much information is shared between two specific values of two

random variables x and y, given the distribution of a third variable Z. We used SPCMI to isolate the information shared between phase front orientation and geomagnetic response from the effect of IMF B_z, which we took as an indicator of dayside and tail reconnection.

3. Results and Discussion

We investigated the connection between solar wind phase front orientation and SME. For each of approximately 300,000 normal - SME pairs, we determined the phase front normal inclination (angle from the GSM XY plane, θ) and azimuth (angle from X in the GSM XY plane, ϕ), and also computed the total angle from the Sun-Earth line. Then, we estimated the probability distributions needed to compute the various informational quantities by computing 2D histograms between the quantities. We evaluated a range of different bin sizes for the histograms in order to maximize resolution while minimizing statistical error. After some trial and error, we settled on histograms with 18 bins to a side, which corresponds to 10 degree bins for phase front angle, and 56 nT bins for SME. Table 1 shows the mutual information and correlation coefficients shared between solar wind phase front inclination, azimuth, angle from Sun-Earth line, IMF B_z, and SuperMAG SME, and the total information (entropy, $\sum p_i \log(p_i)$) contained in each quantity.

The usefulness of mutual information can be seen by comparing phase front azimuth and total phase front angle from the Earth-Sun line. These two quantities are obviously related, as they were computed from the same phase front normal vectors. However, the correlation coefficient between them (shown in Table 1) is very low. The mutual information between them (also shown in Table 1) is very high however, detecting the non-linear connection between the two quantities.

Looking at other values in Table 1, we can see a relatively large correlation between B_z and SME, as expected, which is also seen in the mutual information between the two. However, there is relatively small correlation and mutual information between any of the phase front orientation quantities and SME, other than perhaps correlation between phase front angle and SME. It is hard to pick out any details about how these variables are connected, so we turned to pointwise mutual information. Fig. 3 shows the PMI shared between solar wind phase front azimuth and SME on the left, and between solar wind phase front inclination and SME on the right.

We should note that the scale on these plots range from -0.3 to 0.3 bits, less than that seen in Fig. 1. This means that the effects seen here are roughly an order of magnitude less pronounced than those seen between B_z and SME. The left plot shows that when phase front azimuths lie between 0 and 55 degrees, it is more likely that SME will be high ($>$ 300 nT) than would be expected if the two quantities were independent. Also, SME $>$ 700 nT tends to occur more often when phase front azimuth is near zero. Conversely, it is more likely that SME will be low ($<$ 300 nT) for azimuths outside the above range. On the right, we see a mostly symmetric plot. When solar wind phase front inclination is between -35 and 35 degrees, SME is more likely to be high. Otherwise, SME is more likely to be low. In these cases, the PMI reaches between 0.1 and 0.3. This corresponds to between 1.07 ($2^{0.1}$) and 1.23 ($2^{0.3}$) times more events seen than would be expected if the quantities were independent. This is apparently consistent with the conclusion that radial (oriented towards the Earth) phase front orientations are more geoeffective, and agrees with the results of (Jurac & Richardson, 2001). However, subsequent analysis showed

that the relationships are actually more complicated, as there was a conflating variable (B_z) that needed to be accounted for.

IMF B_z affects both phase front orientation (since it is computed using MVAB-0), and geomagnetic activity (negative B_z results in much more efficient energy transfer through dayside and tail reconnection). Because of this, when we computed the PMI between phase front orientation and SME, some of what was seen was due to certain phase front orientations being more common when B_z was negative. The simplest way to examine this was to split the data set into intervals where $B_z > 0$, and intervals where $B_z < 0$. When we did this and plotted pointwise mutual information for phase front azimuth and inclination vs SME for both cases, we obtained Fig. 4.

Here, we can see a clear difference between mutual information for $B_z > 0$ and $B_z < 0$ events. When $B_z < 0$ (dayside and tail reconnection), we see high mutual information (about 0.2 to 0.3 bits) between high SME (> 500 nT) and low azimuth/inclination (< 45 deg). We also see high mutual information (about 0.3 bits) between low SME and high azimuth/inclination (> 45 deg). On the other hand, when $B_z > 0$ (viscous interaction and high latitude reconnection), we see that there is high mutual information (about 0.3 bits) between high SME, and inclination and azimuth near 0 deg and 45 deg respectively (the average Parker spiral orientation).

We went one step further in isolating the effect of phase front orientation on geomagnetic activity from B_z through summed pointwise conditional mutual information. As detailed in section 2.4, this quantity allows us to remove the information shared between phase front orientation and SuperMAG SME that is also shared with B_z.

Fig. 5 shows SPCMI between the same quantities as in Fig. 3, but with information shared with B_z removed. These two plots now look very similar to what was seen in Fig. 4 for $B_z > 0$. Starting with the left plot, it is clear that times with phase front azimuths around 45 degrees are more likely to also have high SME than would be expected if the two quantities were independent. Examining the relationship between phase front inclination and SME, we see that by removing the influence of B_z, we have removed the low SME being more likely for inclinations away from zero degrees. However, it is still more likely to observe high SME occurring for phase front inclinations near zero.

It should be noted that if we plot SPCMI for only intervals where B_z is negative, we see no structure at all (not shown). This, along with results shown in Fig. 4 indicates that any connection between phase front orientation and geomagnetic activity only exists during times of positive B_z.

We have found that when $B_z > 0$, after accounting for B_z, time intervals with high SME occur more often than would be expected assuming independence when phase fronts are oriented in the average Parker spiral direction. Having removed information due to IMF B_z, this is either caused by the phase front orientation, or there could be another solar wind variable controlling both. We investigated two other possible solar wind quantities that may have been responsible: solar wind speed, and solar wind number density.

The top left plot in Fig. 6 shows PMI between SME and solar wind speed. It indicates that, as one might expect, higher solar wind speeds result in excess higher SME events. Moving to the middle left plot, we see PMI between phase front azimuth and solar wind speed. We can see that low solar wind speed (< 400 km/s) leads to an excess of moderately inclined to nearly frontal (-40 deg $< \phi < 40$ deg) phase front azimuth events, and higher

solar wind speed (> 500 km/s) leads to an excess of large phase front azimuth events ($\phi > 60$ deg, < -60 deg). This is approximately consistent with the Parker spiral model, as that predicts phase front azimuth to increase with increasing solar wind speed. The bottom left plot shows PMI between phase front inclination and solar wind speed. Here the PMI is more faint, and it is harder to see any pattern. Combining the influence of solar wind speed on phase front orientation with its influence on SME, we could posit that nearly frontal phase fronts should contribute to more lower SME events, and obliquely angled phase fronts should contribute to more higher SME events. This contribution is at odds with the result that phase fronts aligned in the average Parker spiral direction are more geoeffective (when $B_z > 0$), and so we can be sure that solar wind speed is not responsible for Parker spiral aligned phase fronts being more geoeffective.

Next we focus on solar wind number density. The plots here are laid out similar to the ones involving solar wind speed, on the fight side of Fig. 6. Starting with the upper right plot, we see PMI between SME and solar wind number density. Though not as coherent as solar wind speed, we also see here that high solar wind density ($> 10\text{cm}^{-3}$ leads to an excess of high SME (> 600 nT). There is not an equivalent excess for low SME, low solar wind density events though. Next we consider the middle right and bottom right plots, showing PMI between phase front azimuth and solar wind density, and phase front inclination and solar wind density respectively. Both of these plots look remarkably similar. There is an excess of head-on phase front azimuth/inclination ($-40 < \phi/\theta < 40$) events for higher solar wind density ($> 5\text{cm}^{-3}$), and an excess of oblique angled azimuth/inclination (-40 deg $< \phi/\theta < 40$ deg) events for low solar wind density ($< 5\text{cm}^{-3}$). If we compare the solar wind density - phase front orientation plots to the

solar wind density - SME plot, we could posit that head-on phase fronts should contribute an excess of high SME events through solar wind density. This also is at odds with the result that Parker spiral aligned phase fronts lead to higher solar wind geoeffectiveness (When IMF $B_z > 0$). This leads us to conclude that those results are not due to the influence of solar wind density.

Having ruled out the most likely conflating variables, one could ask why Parker spiral oriented phase fronts lead to a greater proportion of high levels of geomagnetic activity. We think that the Parker spiral angle itself is not special, and instead we are seeing the effect of stable versus varying phase front angles. Since the Parker spiral orientation is the most common, it is possible that the mechanisms involved in energy transfer during positive B_z (viscous interaction or high latitude reconnection) are more efficient when the solar wind impacts the magnetosphere in the same place over time. We explored this possibility by plotting the mutual information between the change in phase front azimuth and inclination over the previous 12 hours and SuperMAG SME, as pictured in Fig. 7. What we see here is that smaller changes in phase front orientation (< 40 deg) share more information with higher SME than larger changes in both phase front azimuth and inclination. We should note that the scale for these plots ranges from -0.15 bits to 0.15 bits, half that seen in the other PMI plots concerning SME (Figures 3, 4, and 5), meaning this effect is on average smaller than those. In other words, when phase front orientation is essentially constant, we tend to see higher SME about 10% more than we would expect if phase front orientation and SME were independent. This suggests that phase fronts impacting the magnetosphere at the same angle (meaning impacting the same part of the magnetosphere) over time can result in more efficient transfer energy into the

magnetosphere through either viscous interaction or high latitude reconnection into the magnetosphere. There are many possible mechanisms by which this could happen. If this phenomenon is related to viscous interaction, it could be because phase planes impacting the magnetosphere in the same place set up more stable flow patterns than if phase planes vary. Alternatively, if this phenomenon is related to high latitude reconnection, perhaps high latitude reconnection is more efficient the longer it goes on in the same place. A possible next step would be to try to determine which mechanism is responsible for this effect.

4. Conclusions

We performed an information theoretic analysis with almost two decades of solar wind and ground magnetometer observations in order to explore the effect of solar wind phase front orientation on the subsequent geomagnetic activity resulting from the interaction between the solar wind and the magnetosphere. We found that, in general, phase fronts with radial normals are more geoeffective than those with normals inclined away from the Earth-Sun line. However, this seems to be because phase fronts with radial normals are more prevalent when dayside and tail reconnection is occurring.

We controlled for the influence of these kinds of reconnection by controlling for B_z using summed pointwise conditional mutual information. This led to the result that during times of positive IMF B_z, phase fronts oriented along the average Parker spiral direction lead to more high geomagnetic activity than would be expected if the two quantities were unrelated. We then ruled out solar wind density or speed causing this. Because the average Parker spiral orientation is most common, we theorize this effect is related to the constancy of solar wind phase front orientation over time. A constant phase front

orientation may result in more effective viscous coupling between the solar wind and magnetosphere, or in more efficient energy transfer due to high latitude reconnection. The mutual information between change in phase front azimuth over previous time and SuperMAG SME (Fig. 7) lends this credence. This result is not the same as what was found for shocks. This could be because of the different energy scales and energy transfer mechanisms involved.

We also conclude by noting the usefulness of using pointwise informational quantities to explore connections between variables. The large amount of accumulated data about the geomagnetic field and near earth space is especially well suited for information analysis. In the future, it would be useful to look further into the temporal aspect of the phase front angle - geomagnetic activity connection. This could make it clear whether what we are seeing is really related to the constancy of phase front orientation or not, and could be done by looking at mutual information between time-shifted versions of these variables. Additionally, trying to relate the constancy of phase front orientation to high latitude reconnection and viscous interaction using information theory could help to determine which mechanism is responsible for steady phase front orientation being more geoeffective.

Acknowledgments. This work was supported by Canadian Space Agency Geospace Observation grant 14SUGOCGV. It was also supported by a NSERC Postgraduate Scholarship. D.M.O. acknowledges the NASA-SR grants 13-SRITM13 2-0011 and HSR-MAG14 2-0062 under contract with UMBC. We gratefully acknowledge the SuperMAG collaborators (`http://supermag.jhuapl.edu/info/?page=acknowledgement`). The ACE data used in this study can be found at the Coordinated Data Analysis Web (`http://cdaweb.gsfc.nasa.gov`).

Références

Axford, W. I. (1964). Viscous interaction between the solar wind and the earth's magnetosphere. *Planetary and Space Science*, *12*(1), 45–53. 10.1016/0032-0633(64)90067-4

Cameron, T., & Jackel, B. (2016). Quantitative evaluation of solar wind time-shifting methods. *Space Weather*, 973–981. 10.1002/2016SW001451

Chen, J., Sharma, A. S., Edwards, J. W., Shao, X., & Kamide, Y. (2008). Spatiotemporal dynamics of the magnetosphere during geospace storms : Mutual information analysis. *Journal of Geophysical Research*, *113*(January 2007), 1–15. 10.1029/2007JA012310

Collier, M. R., Szabo, A., Slavin, J. A., & Lepping, R. P. (2000). IMF length scales and predictability : The two length scale medium. *International Journal of Geomagnetism and Aeronomy*, *2*(1), 3–16.

Crooker, N. U. (1992). Reverse Convection. *J. Geophys. Res.*, *97*(A12), 19363–19372. 10.1029/92ja01532

Davis, T. N., & Sugiura, M. (1966). Auroral electrojet activity index AE and its universal time variations. *J. Geophys. Res.*, *71*(3), 785-801. 10.1029/JZ071i003p00785

Gjerloev, J. W. (2012). The SuperMAG data processing technique. *J. Geophys. Res.*, *117*(A09213), 1–19. 10.1029/2012JA017683

Gjerloev, J. W., Hoffman, R. A., Friel, M. M., Frank, L. A., & Sigwarth, J. B. (2004). Substorm behavior of the auroral electrojet indices. *Ann. Geophys.*, *22*(6), 2135–2149. 10.5194/angeo-22-2135-2004

Guo, X.-C., Hu, Y.-Q., & Wang, C. (2005). Earth's magnetosphere impinged by interplanetary shocks of different orientations. *Chinese Phys. Lett.*, *22*(12), 3221-3224.

10.1088/0256-307X/22/12/067

Johnson, J. R., & Wing, S. (2014). External versus internal triggering of substorms : An information-theoretical approach. *Geophysical Research Letters*, 5748–5754. 10.1002/2014GL060928.Received

Jurac, S., & Richardson, J. D. (2001). The dependence of plasma and magnetic field correlations in the solar wind on geomagnetic activity by four spacecraft. *Journal of Geophysical Research*, *106*, 29195–29205. 10.1029/2000JA000180

Kilpua, E. K. J., Lumme, E., Andreeova, K., Isavnin, A., & Koskinen, H. E. J. (2015). Properties and drivers of fast interplanetary shocks near the orbit of the Earth (1995-2013). *J. Geophys. Res. Space Physics*, *120*(6), 4112–4125. 10.1002/2015JA021138

Lepping, R. P., Wu, C. C., & McCleman, K. (2003). Two-dimensional curvature of large angle interplanetary MHD discontinuity surfaces: IMP-8 and WIND observations. *Journal of Geophysical Research: Space Physics*, *108*(A7), 1–20. 10.1029/2002JA009640

Lizier, J. T. (2014). Measuring the Dynamics of Information Processing on a Local Scale in Time and Space. In M. Wibral, R. Vicente, & J. T. Lizier (Eds.), *Directed information measures in neuroscience* (pp. 161–193). Berlin, Heidelberg : Springer Berlin Heidelberg. 10.1007/978-3-642-54474-3$_7$

Lu, J. Y., Jing, H., Liu, Z. Q., Kabin, K., & Jiang, Y. (2013). Energy transfer across the magnetopause for northward and southward interplanetary magnetic fields. *Journal of Geophysical Research: Space Physics*, *118*(5), 2021–2033. 10.1002/jgra.50093

Mailyan, B., Munteanu, C., & Haaland, S. (2008). What is the best method to calculate the solar wind propagation delay? *Ann. Geophys.*, *26*(8), 2383–2394. 10.5194/angeo-

26-2383-2008

Newell, P. T., & Gjerloev, J. W. (2011a). Evaluation of SuperMAG auroral electrojet indices as indicators of substorms and auroral power. *J. Geophys. Res.*, *116*(A12). 10.1029/2011JA016779

Newell, P. T., & Gjerloev, J. W. (2011b). Substorm and magnetosphere characteristic scales inferred from the SuperMAG auroral electrojet indices. *J. Geophys. Res.*, *116*(A12211), 1-12. 10.1029/2011JA016936

Oliveira, D. M., Arel, D., Raeder, J., Zesta, E., Ngwira, C. M., Carter, B. A.Gjerloev, J. W. (2018). Geomagnetically Induced Currents Caused by Interplanetary Shocks With Different Impact Angles and Speeds. *Space Weather*, *16*(6), 636–647. 10.1029/2018SW001880

Oliveira, D. M., & Raeder, J. (2014). Impact angle control of interplanetary shock geoeffectiveness. *J. Geophys. Res. Space Physics*, *119*(10), 8188–8201. 10.1002/2014JA020275

Oliveira, D. M., & Raeder, J. (2015). Impact angle control of interplanetary shock geoeffectiveness: A statistical study. *J. Geophys. Res. Space Physics*, *120*(6), 4313-4323. 10.1002/2015JA021147

Oliveira, D. M., Raeder, J., Tsurutani, B. T., & Gjerloev, J. W. (2016). Effects of interplanetary shock inclinations on nightside auroral power intensity. *Braz. Jour. Phys.*, *46*(1), 97–104. 10.1007/s13538-015-0389-9

Oliveira, D. M., & Samsonov, A. A. (2018). Geoeffectiveness of interplanetary shocks controlled by impact angles: A review. *Advances in Space Research*, *61*(1), 1–44. 10.1016/j.asr.2017.10.006

Parker, E. N. (1965). Dynamical Theory of the Solar Wind. *Space Science Reviews*, *4*, 666–708.

Prichard, D., Borovsky, J. E., Lemons, P. M., & Price, C. P. (1996). Time dependence of substorm recurrence: An information-theoretic analysis. *Journal of Geophysical Research*, *101*, 15,359–15,369. 10.1029/95JA03419

Samsonov, A. A., Sergeev, V. A., Kuznetsova, M. M., & Sibeck, D. G. (2015). Asymmetric magnetospheric compressions and expansions in response to impact of inclined interplanetary shock. *Geophys. Res. Lett.*, *42*(12), 4716–4722. 10.1002/2015GL064294

Selvakumaran, R., Veenadhari, B., Ebihara, Y., Kumar, S., & Prasad, D. S. V. V. D. (2017). The role of interplanetary shock orientation on SC/SI rise time and geoeffectiveness. *Adv. Space Res.*, *59*(5), 1425–1434. 10.1016/j.asr.2016.12.010

Sonnerup, B., & Scheible, M. (1998). Minimum and maximum variance analysis. In G. Paschmann & P. W. Daly (Eds.), *Analysis methods for multi-spacecraft data* (pp. 185–220). Bern : International Space Science Institute.

Takeuchi, T., Russell, C. T., & Araki, T. (2002). Effect of the orientation of interplanetary shock on the geomagnetic sudden commencement. *J. Geophys. Res.*, *107*(A12), 1423. 10.1029/2002JA009597

Wang, C., Li, C. X., Huang, Z. H., & Richardson, J. D. (2006). Effect of interplanetary shock strengths and orientations on storm sudden commencement rise times. *Geophys. Res. Lett.*, *33*(L14104), 1–3. 10.1029/2006GL025966

Wyner, A. D. (1978). A definition of conditional mutual information for arbitrary ensembles. *Information and Control*, *38*(1), 51–59. 10.1016/S0019-9958(78)90026-

Table 1. Table of entropy ($\sum p_i \log(p_i)$), mutual information, and correlation values. The top right (white) cells show mutual information between quantities, the bottom left (light grey) cells show correlation between quantities, while the diagonal (dark grey) cells show total entropy for each quantity. Here, azimuth refers to angle from the Earth-Sun line on the ecliptic, inclination refers to the angle off the ecliptic, and angle simply refers to total angle from the Earth-Sun line.

	PF Azimuth	PF Inclination	PF Angle	IMF B_z	SME
PF Azimuth	3.15196	0.02810	0.84894	0.02391	0.00383
PF Inclination	-0.0215	3.15274	0.51067	0.07435	0.00585
PF Angle	0.02964	-0.0081	3.14472	0.07516	0.00669
IMF B_z	0.00387	-0.0142	0.00138	2.42733	0.15701
SME	0.00475	-0.0007	-0.0784	-0.3537	2.86224

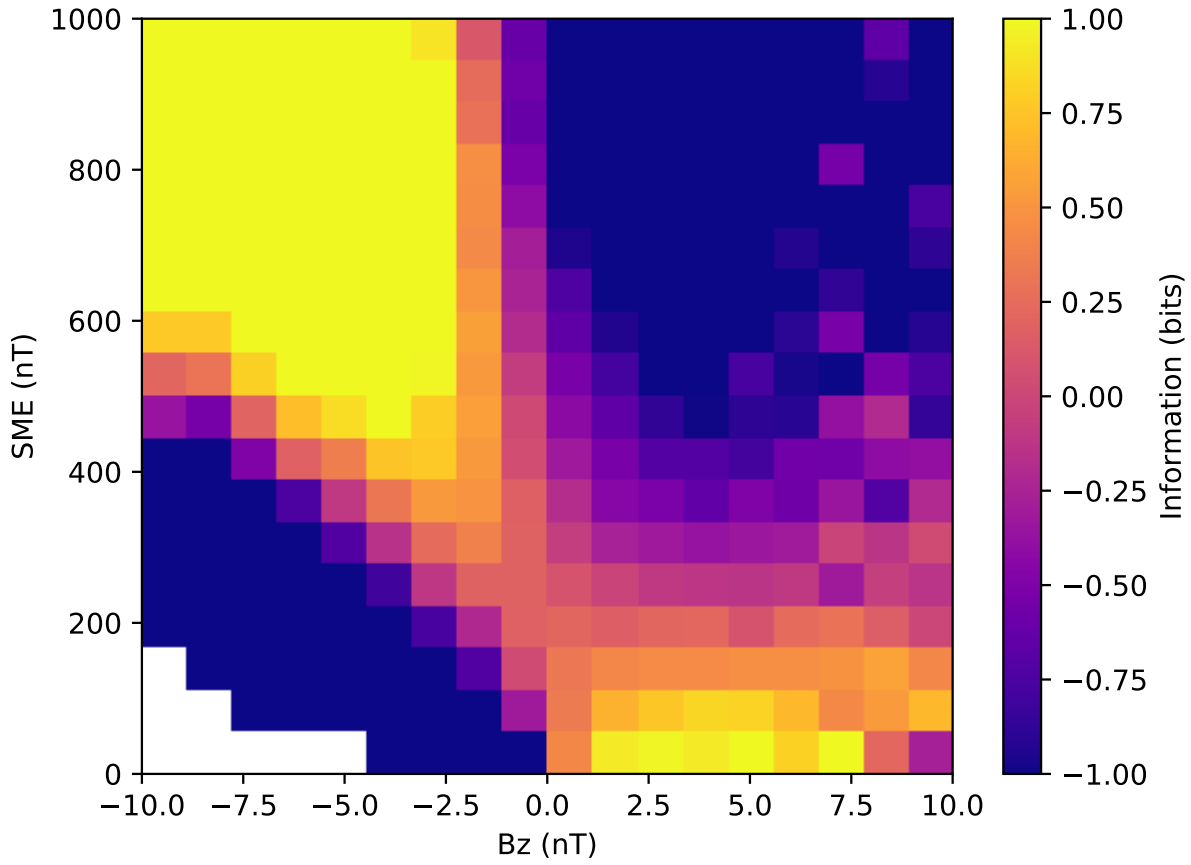

Figure 1. Pointwise mutual information shared between IMF B_z and SuperMAG SME. The PMI reaches higher than 1 in some places (high SME, $B_z < 0$ and low SME, $B_z > 0$), and lower than -1 in others (low SME, $B_z < 0$ and high SME, $B_z > 0$). This illustrates the usefulness of pointwise versions of informational quantities.

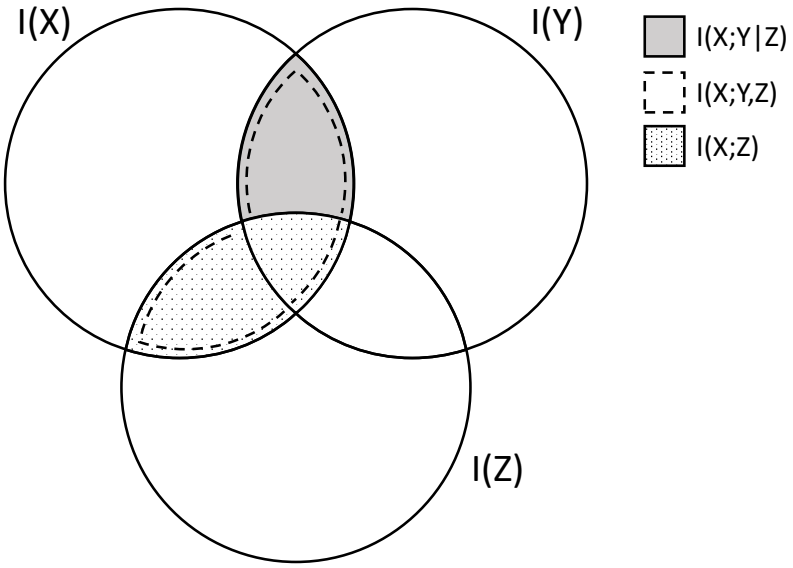

Figure 2. Quantities needed to calculate conditional mutual information between X and Y given Z. Each circle represents the total information contained in X, Y, or Z. The dotted region represents the information shared between X and Z, the region surrounded by the dashed line represents the information shared between X and the combination of Y and Z, while the dark shaded intersection shows conditional mutual information between X and Y given Z. Note that it does not include any information contained in Z.

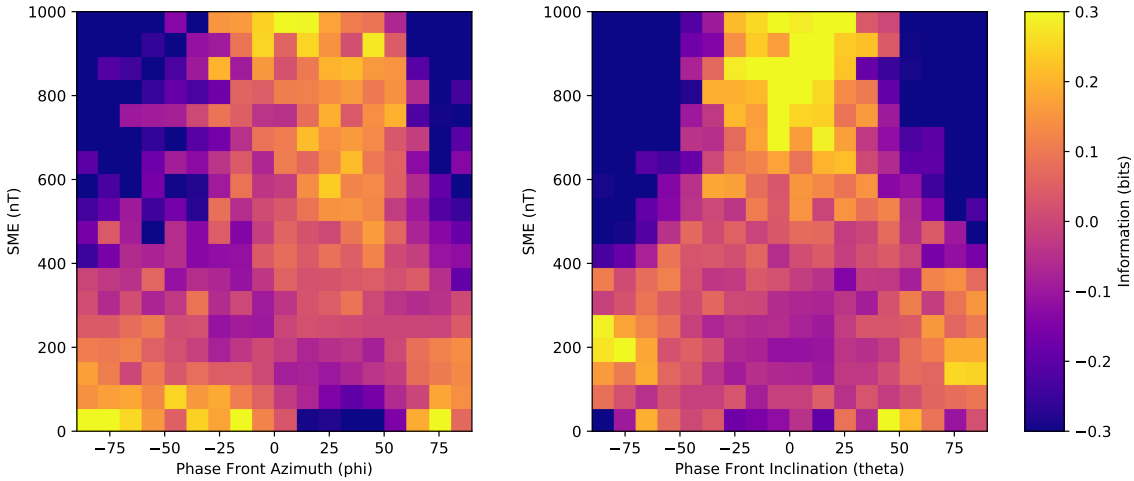

Figure 3. (left) Pointwise mutual information shared between solar wind phase front azimuth and SuperMAG SME. (right) Pointwise mutual information shared between solar wind phase front inclination and SuperMAG SME.

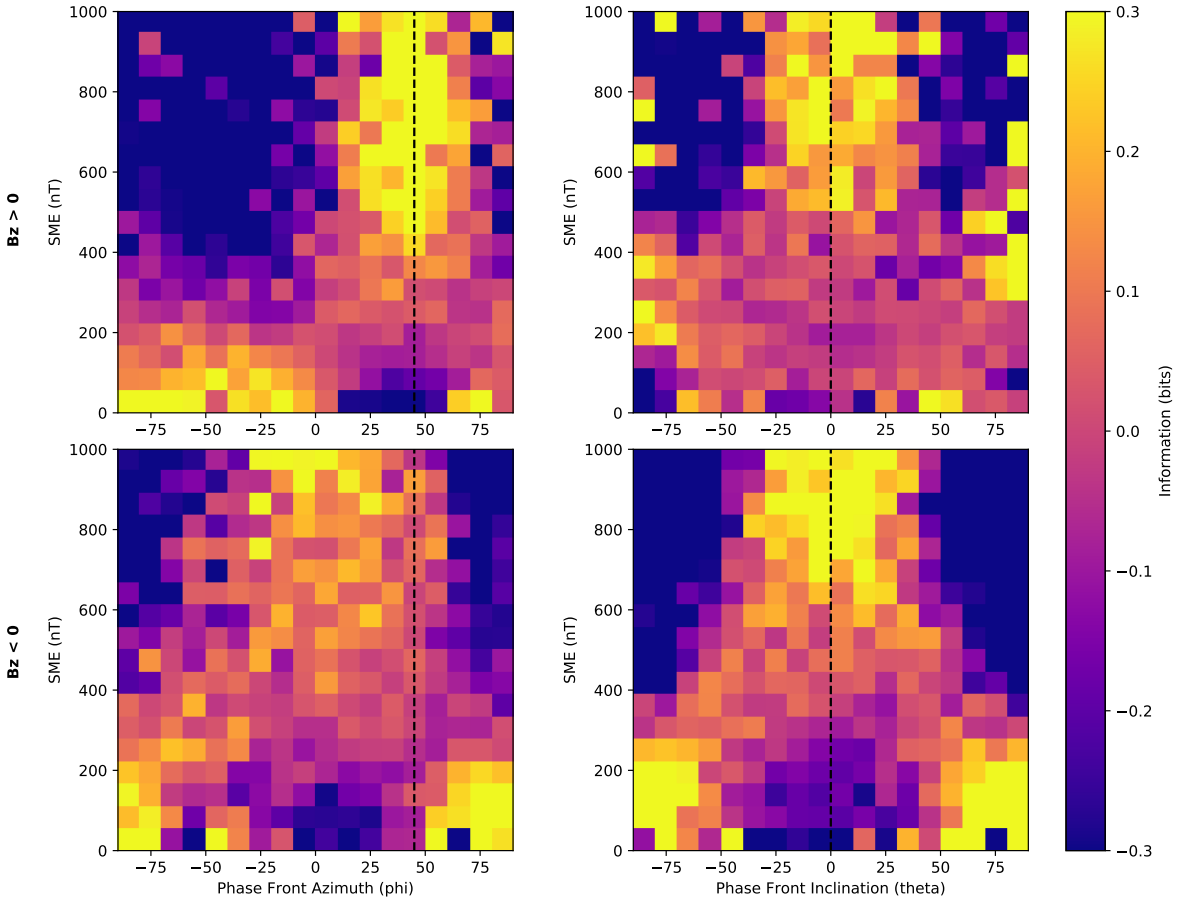

Figure 4. Pointwise mutual information shared between solar wind phase front Azimuth (left) or Inclination (right) and SuperMAG SME. The top plots show this only for events where $B_z > 0$, whereas the bottom plots show this for only events where $B_z < 0$. The dashed line in the plots shows the average Parker spiral orientation (45 degrees azimuth, 0 degrees inclination).

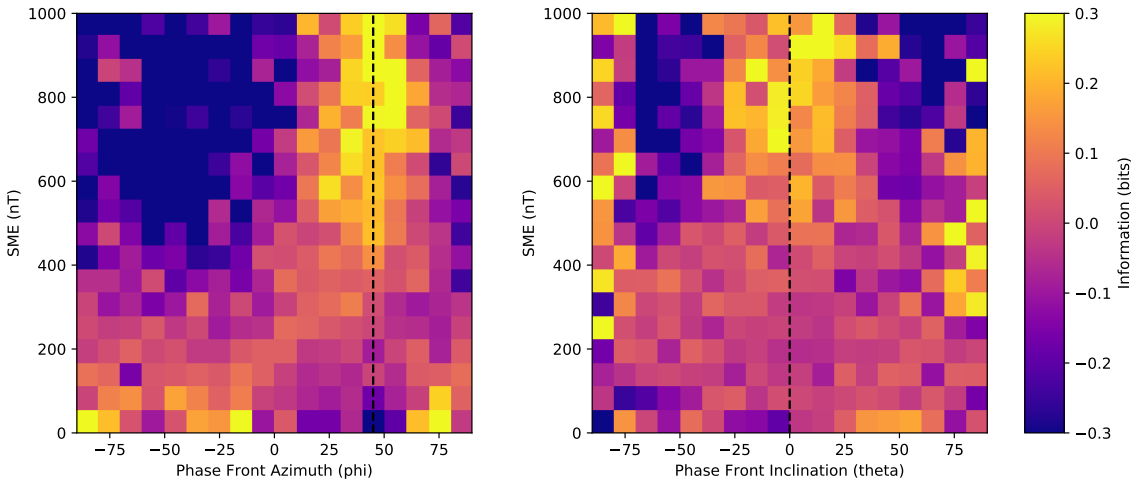

Figure 5. (left) Summed pointwise conditional mutual information shared between solar wind phase front Azimuth and SuperMAG SME, given B_z. (right) Summed pointwise conditional mutual information shared between solar wind phase front inclination and SuperMAG SME, given B_z. The dashed line in the plots shows the average Parker spiral orientation (45 degrees azimuth, 0 degrees inclination).

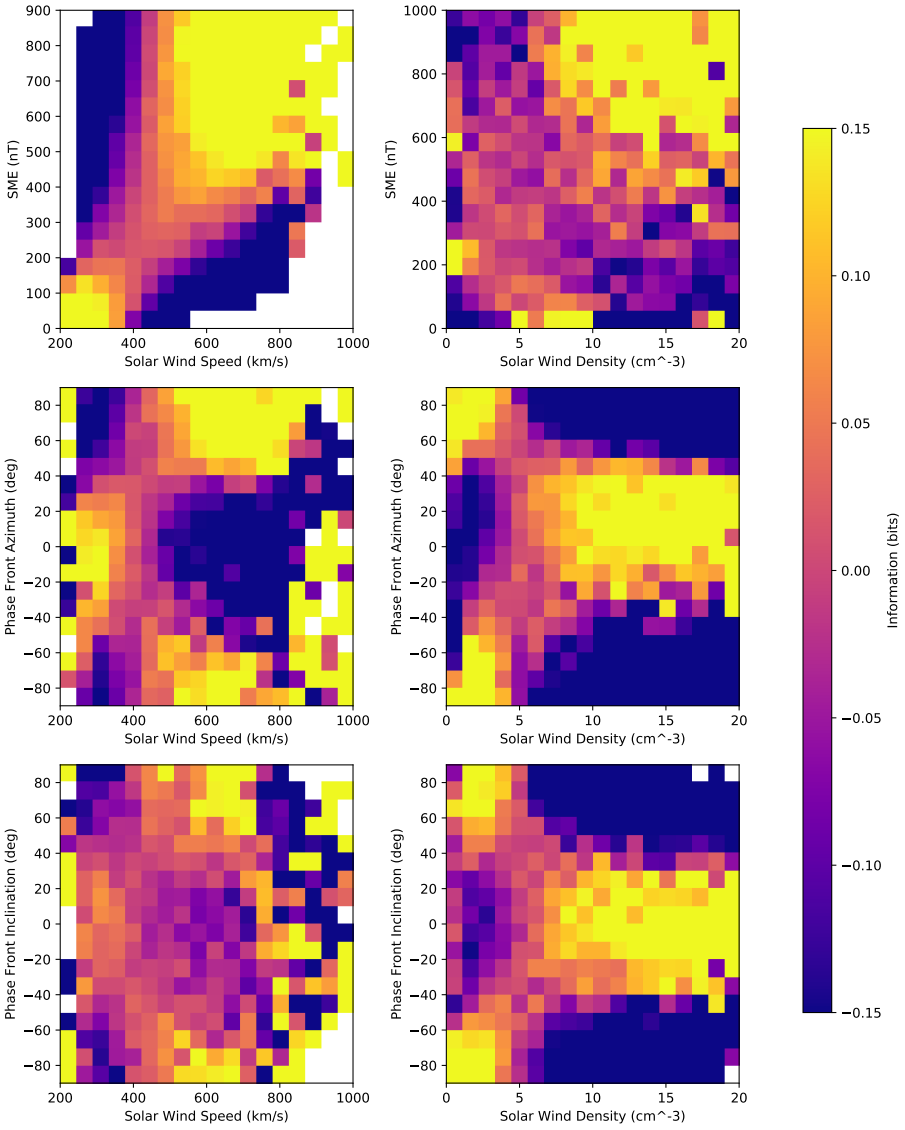

Figure 6. (left) Pointwise mutual information plots concerning solar wind speed. From the top, pointwise mutual information between solar wind speed and SME, solar wind speed and solar wind phase front azimuth, solar wind speed and solar wind phase front inclination. (right) Pointwise mutual information plots concerning solar wind density. From the top, pointwise mutual information between solar wind density and SME, solar wind density and solar wind phase front azimuth, solar wind density and solar wind phase front inclination.

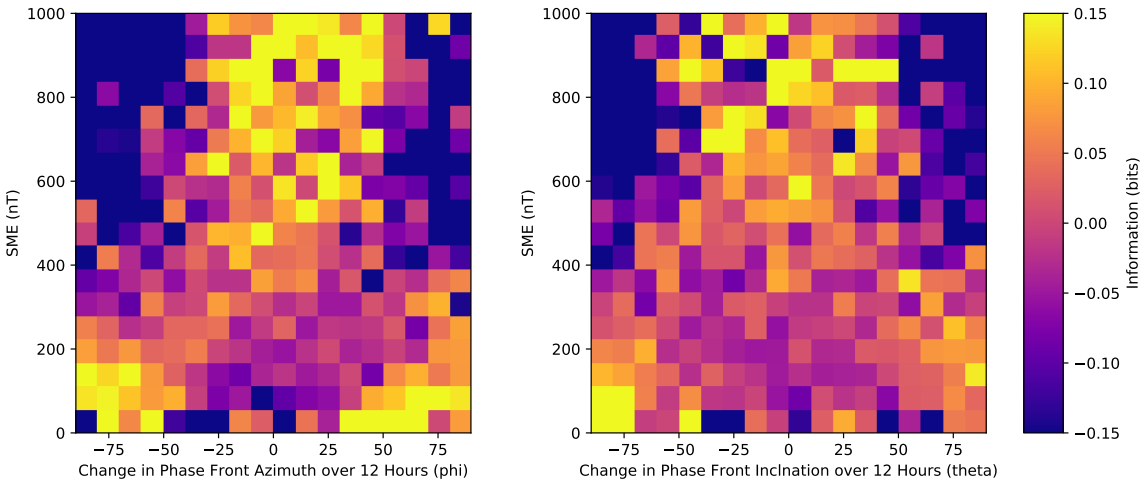

Figure 7. (left) Pointwise Mutual information between SuperMAG SME and the change in solar wind phase front azimuth over the previous 12 hours. (right) Pointwise Mutual information between SuperMAG SME and the change in solar wind phase front inclination over the previous 12 hours. Note that the scale here is half that of the above PMI plots concerning SME (Figures 3, 4, and 5).